Supplementary Materials to

Paleogeographic controls on the evolution of Late Cretaceous ocean circulation

Jean-Baptiste Ladant, Christopher J. Poulsen, Frédéric Fluteau, Clay R. Tabor,
Kenneth G. MacLeod, Ellen E. Martin, Shannon J. Haynes, Masoud A. Rostami

Table S1-S3.

Supplementary Figures S1-S19.

	Cenomanian				Maastrichtian			
Total runoff supply (mSv) Total basin area (10^6 km^2)	Pacific	Atlantic	Indian	Indo-Atlantic	Pacific	Atlantic	Indian	Indo-Atlantic
Global	833 221.84	560 41.71	647 71.39	1207 113.1	792 212.27	853 58.08	648 69.01	1501 127.09
Southern Hemisphere high-latitudes	130 19.95	54 5.59	195 8.03	249 13.62	129 17.61	55 9.27	211 11.11	266 20.38
Northern Hemisphere high-latitudes	130 15.49	83 2.61	0 0	83 2.61	169 15.04	151 3.17	0 0	151 3.17
Mid- and low-latitudes	573 186.4	423 33.5	452 63.36	875 96.86	494 179.62	647 45.64	436 57.9	1083 103.54

Table S1. Total runoff freshwater supply (mSv) for the Cenomanian and Maastrichtian simulations. The Pacific, Atlantic and Indian basins are defined as shown on Fig. S3. Southern and northern high-latitudes are defined as latitudes < 50°S and > 50°N respectively.

Site	Location	Paleolatitude	Paleolongitude	Paleodepth (m)	Average ε_{Nd}	References
765	Argo Abyssal Plain	40°S	105°E	5000	–7.9	MT12, GL92
763	Central Exmouth Plateau	44°S	100°E	500	–9.8	LH12, MT12, V13, GL92
766	Gascoyne Abyssal Plain	45°S	95°E	3000	–6.8	R10, MT12, GL92
258	Naturaliste Plateau	57°S	85°E	2500 – 3000	–8.0	M16
1135	Southern Kerguelen Plateau	55°S	72°E	1300 – 2000	–7.9	LH12
1138	Kerguelen Plateau	52°S	70°E	500 – 1500	–5.6	MT12
551	Goban Spur	40°N	2°W	1500	–7.1	M12, M85
530	SE Angola Basin	30°S	4°W	> 2000	–7.5	R10
530	SE Angola Basin	31°S	5°W	3000	–7.7	MT13
361	Cape Basin	45°S	5°W	4000	–6.1	MT13
367	Cape Verde	17°N	18°W	> 2000	–9.0	M12
700	East Georgia Basin	52°S	18°W	1500 – 2000	–7.7	M16
1276	Newfoundland Margin	35°N	22°W	> 2000	–6.8	RV12
511	Falkland Plateau	54°S	25°W	> 1000	–5.2	R10
511	Falkland Basin	52°S	26°W	1800	–5.1	MT13
1261	Demerara Rise	6°N	29°W	1000 – 1500	–13.0	M12
1260	Demerara Rise	8°N	31°W	1000 – 1500	–13.5	ML08, ML11, M12, JB10
1258	Demerara Rise	9°N	32°W	1000 – 1500	–13.5	ML08, ML11, M12, JB10
386	Bermuda Rise	27°N	35°W	> 2000	–6.8	M12, RV12
1050	Blake Nose	26°N	42°W	1000 – 2000	–5.2	M12
1208	Shatsky Rise	15°N	154°W	1500 – 2000	–3.4	MT12

Table S2. Cenomanian ε_{Nd} compilation based on Moiroud et al. (2016). The ε_{Nd} values are averaged between 100 Ma and 90 Ma (see main text). GL92: Gradstein and Ludden (1992), JB10: Jiménez Berrocoso et al. (2010), LH12: Le Houedec et al. (2012), M12: Martin et al. (2012), M16: Moiroud et al. (2016), M85: Masson et al. (1985), ML08: MacLeod et al. (2008), ML11: MacLeod et al. (2011), MT12: Murphy and Thomas (2012), MT13: Murphy and Thomas (2013), R10: Robinson et al. (2010), RV12: Robinson and Vance (2012), V13: Voigt et al. (2013).

Site	Location	Paleolatitude	Paleolongitude	Paleodepth (m)	Average ε_{Nd}	References
765	Argo Abyssal Plain	40°S	105°E	5000	–10.2	MT12, GL92
762	Central Exmouth Plateau	44°S	100°E	750	–11.0	LH12, V13, GL92
766	Gascoyne Abyssal Plain	46°S	98°E	3000	–9.4	R10, MT12, GL92
1135	Southern Kerguelen Plateau	58°S	72°E	1300 – 2000	–9.6	LH12
1138	Kerguelen Plateau	55°S	70°E	500 – 1500	–8.5	MT12
758	Ninetyeast Ridge	47°S	50°E	1500 – 2000	–10.3	LH12
530	SE Angola Basin	30°S	1°W	> 2000	–10.0	R10
551	Goban Spur	37°N	5°W	2100	–9.9	M12, M85
690	Maud Rise	65°S	6°W	1800	–9.8	V13
525	Walvis Ridge	36°S	8°W	1000 – 1500	–3.5	V13
367	Cape Verde	15°N	20°W	> 2000	–13.4	M12
700	East Georgia Basin	52°S	20°W	1500 – 2000	–8.2	M16
1276	Newfoundland Margin	35°N	22°W	> 2000	–6.6	RV12
357	Rio Grande Rise	34°S	25°W	1500	–9.7	MT13
511	Falkland Plateau	54°S	29°W	> 1000	–8.7	R10
1261	Demerara Rise	3°N	29°W	1000 – 1500	–15.9	ML11, M12
1260	Demerara Rise	5°N	31°W	1000 – 1500	–15.2	ML08, ML11, M12
1258	Demerara Rise	6°N	32°W	1000 – 1500	–14.8	ML08, ML11, M12
386	Bermuda Rise	26°N	40°W	> 2000	–9.5	M12, RV12
1050	Blake Nose	30°N	54°W	1000 – 2000	–8.5	M12
152	Nicaraguan Rise	15°N	70°W	1500 – 2000	–5.7	M16
323	Bellingshausen Plateau	67°S	100°W	2000	–3.8	T14
596	South Pacific	45°S	120°W	5000	–5.6	T14
1186	Ontong-Java Plateau	15°S	132°W	2800	–5.1	H19
465	Southern Hess Rise	8°N	138°W	900	–3.8	H12
464	Northern Hess Rise	12°N	140°W	4000	–5.1	H12
883	Detroit Seamount	34°N	140°W	2000	2.4	H12, DT04
886	Chinook Trough	30°N	140°W	> 4400	–4.2	ML08
463	Mid-Pacific Mountains	5°S	145°W	1500 – 2000	–5.0	H19

1208	Shatsky Rise	15°N	154°W	3300	–4.0	H12
1209	Shatsky Rise	12°N	158°W	2000 – 3000	–4.3	T04, F05
1210	Shatsky Rise	10°N	160°W	2000 – 3000	–4.3	F05
1211	Shatsky Rise	8°N	162°W	2900	–4.2	T04

Table S3. Maastrichtian ε_{Nd} compilation based on Moiroud et al. (2016). The ε_{Nd} values are averaged between 75 Ma and 65 Ma (see main text). DT04: Doubrovine and Tarduno (2004), F05: Frank et al. (2005), GL92: Gradstein and Ludden (1992), H12: Hague et al. (2012), H19: Haynes et al. (2019) in review, LH12: Le Houedec et al. (2012), M12: Martin et al. (2012), M16: Moiroud et al. (2016), M85: Masson et al. (1985), ML08: MacLeod et al. (2008), ML11: MacLeod et al. (2011), MT12: Murphy and Thomas (2012), MT13: Murphy and Thomas (2013), R10: Robinson et al. (2010), RV12: Robinson and Vance (2012), T04: Thomas (2004), T14: Thomas et al. (2014), V13: Voigt et al. (2013).

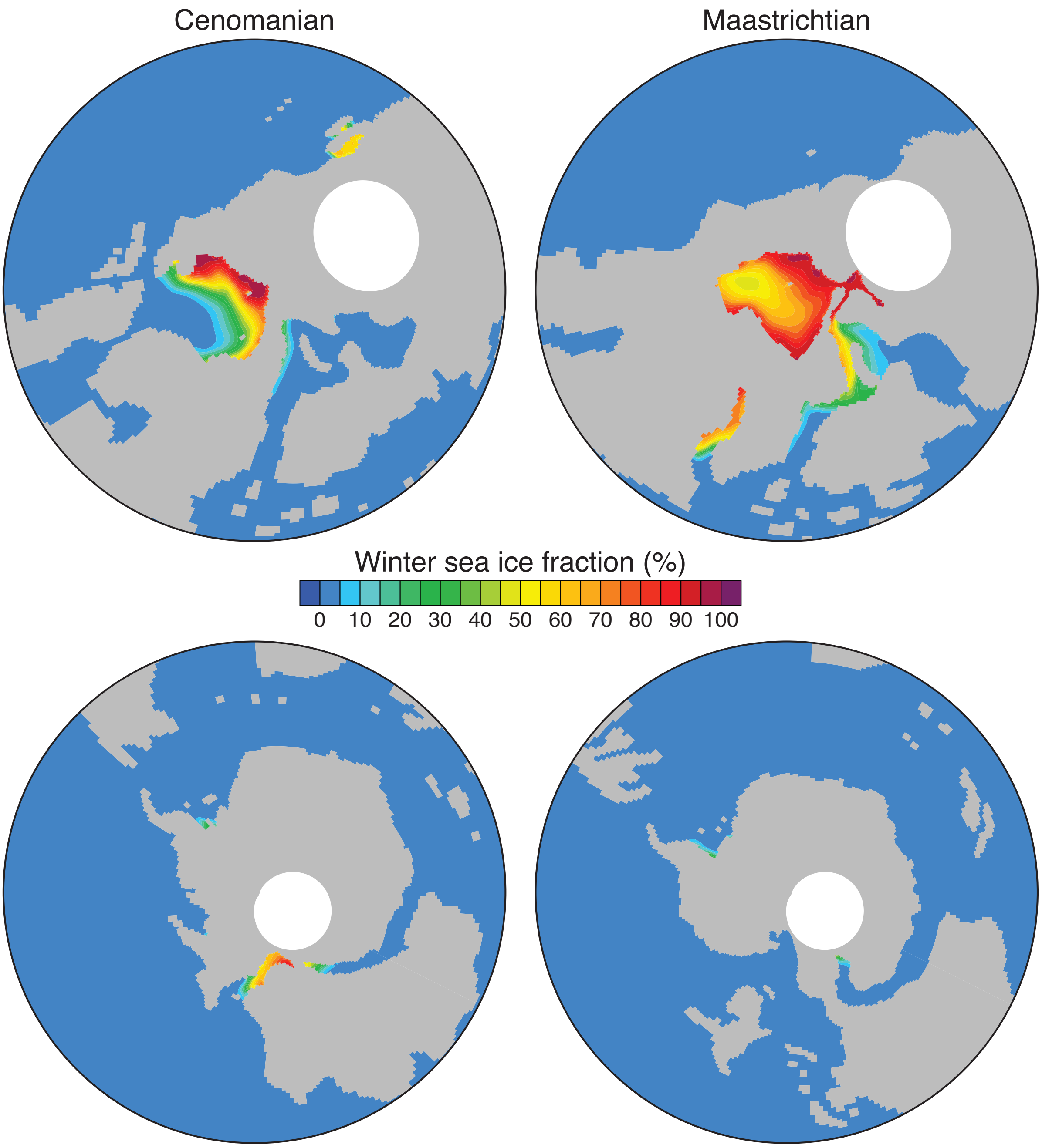

Figure S1. Mean winter sea ice fraction in the Cenomanian and Maastrichtian simulations.

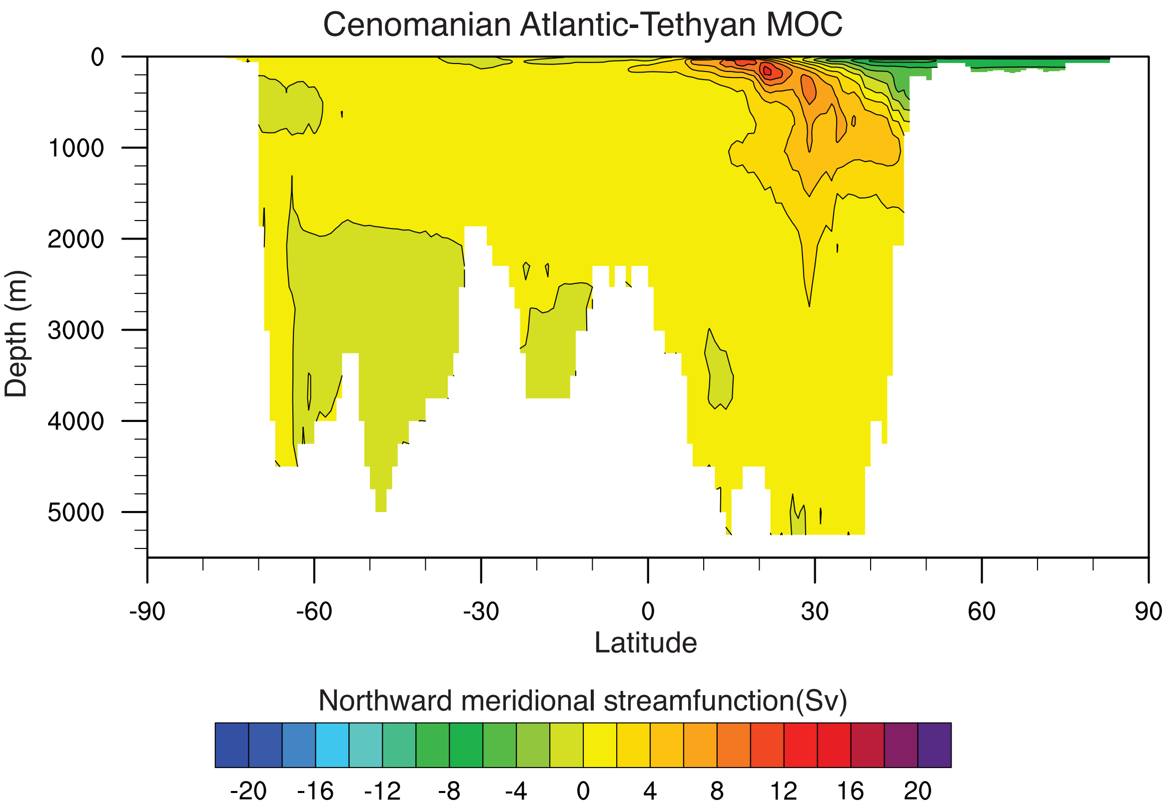

Figure S2. Meridional Overturning Circulation (Sv) in the Atlantic-Tethyan basin of the Cenomanian simulation (Fig. S3).

19

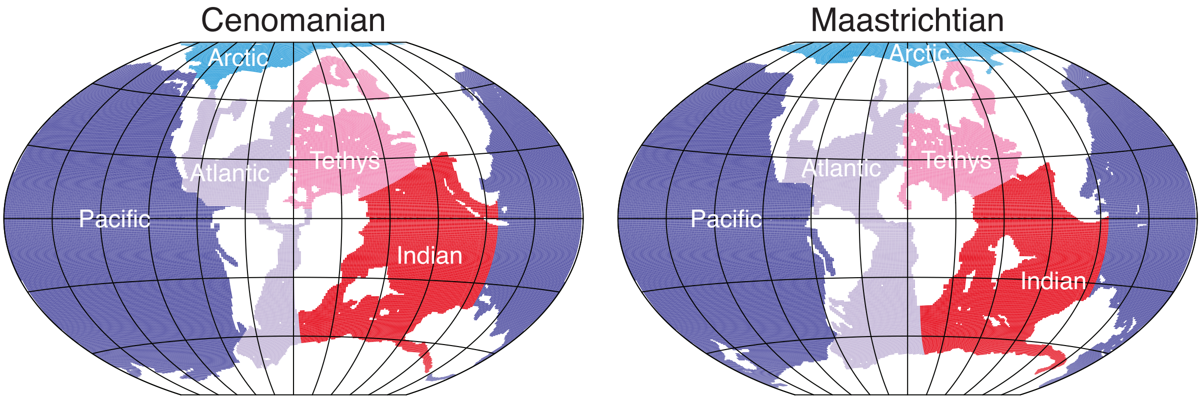

Figure S3. Configuration of the basin mask used in each simulation.

20

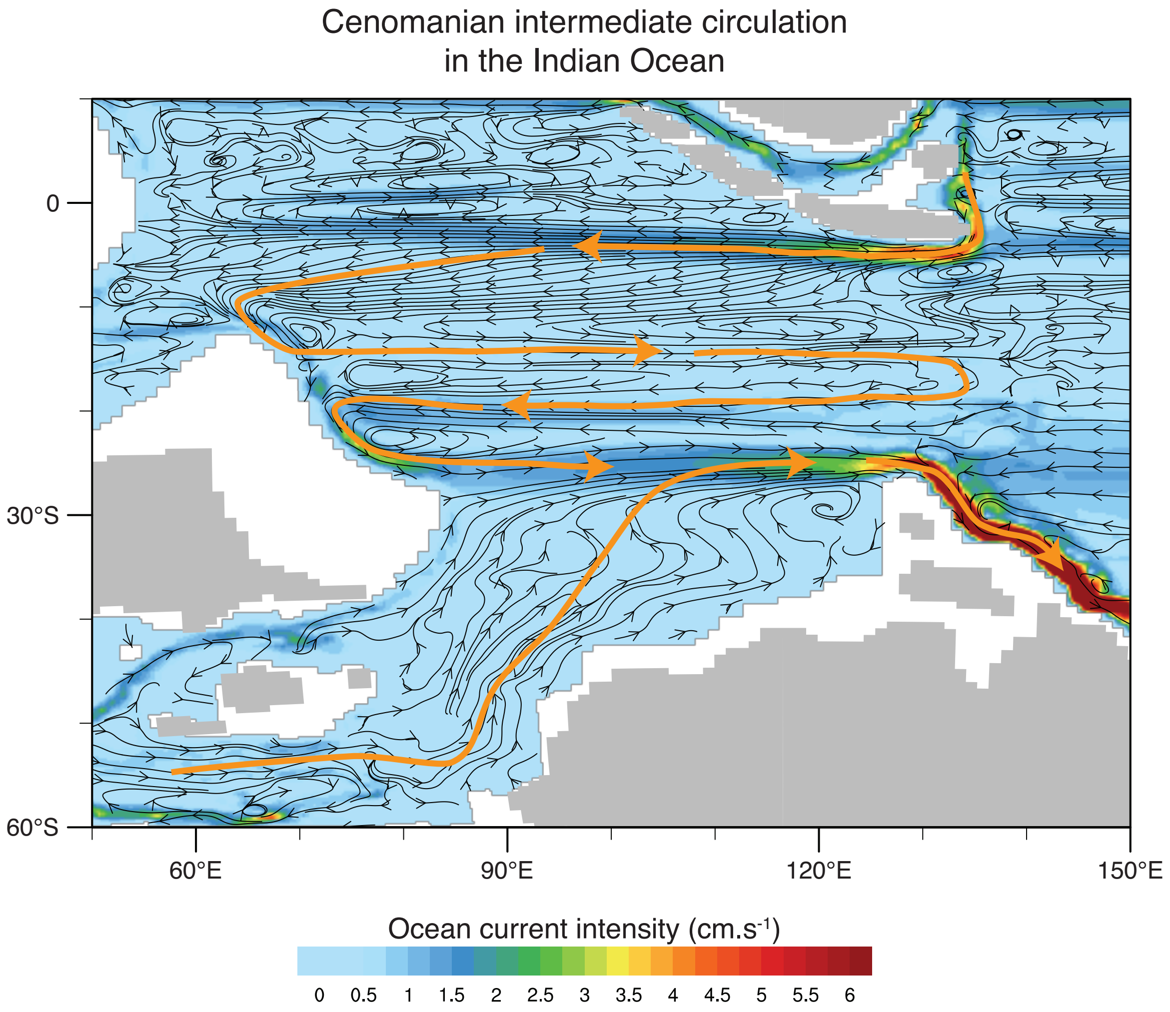

Figure S4. Cenomanian intermediate circulation (1000 m) in the Indian Ocean. Orange arrows represent major intermediate current systems in the Indian Ocean.

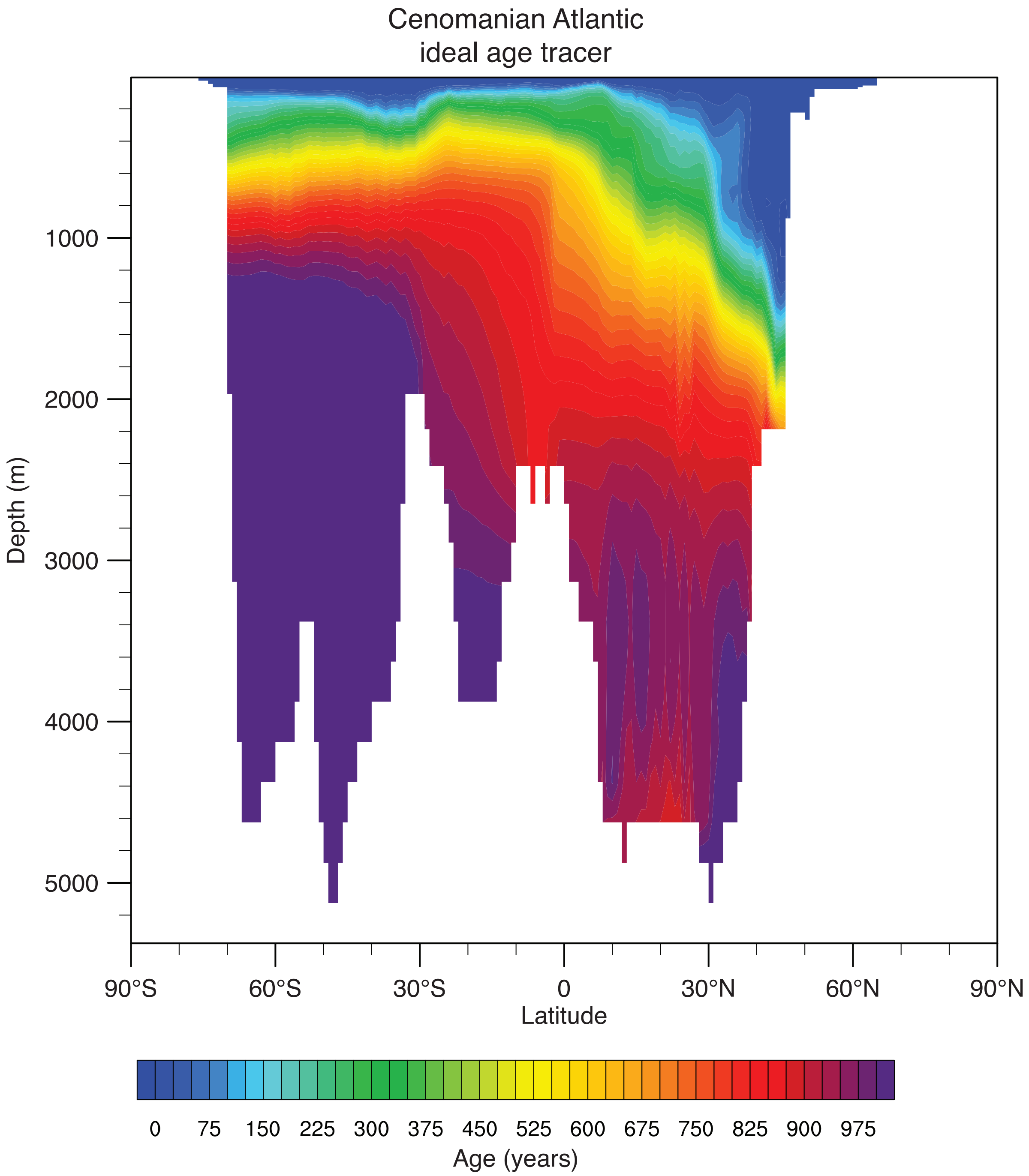

Figure S5. Cenomanian annual mean ideal age tracer in the Atlantic basin.

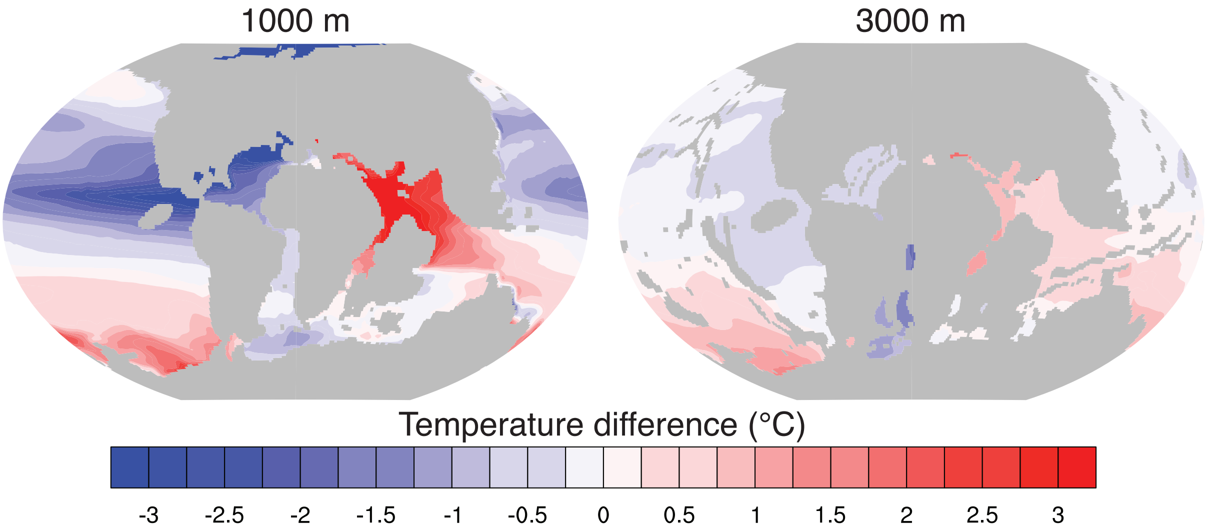

Figure S6. Intermediate (~1000 m) and deep (~3000 m) ocean temperature difference (°C) between the Maastrichtian and the Cenomanian simulations.

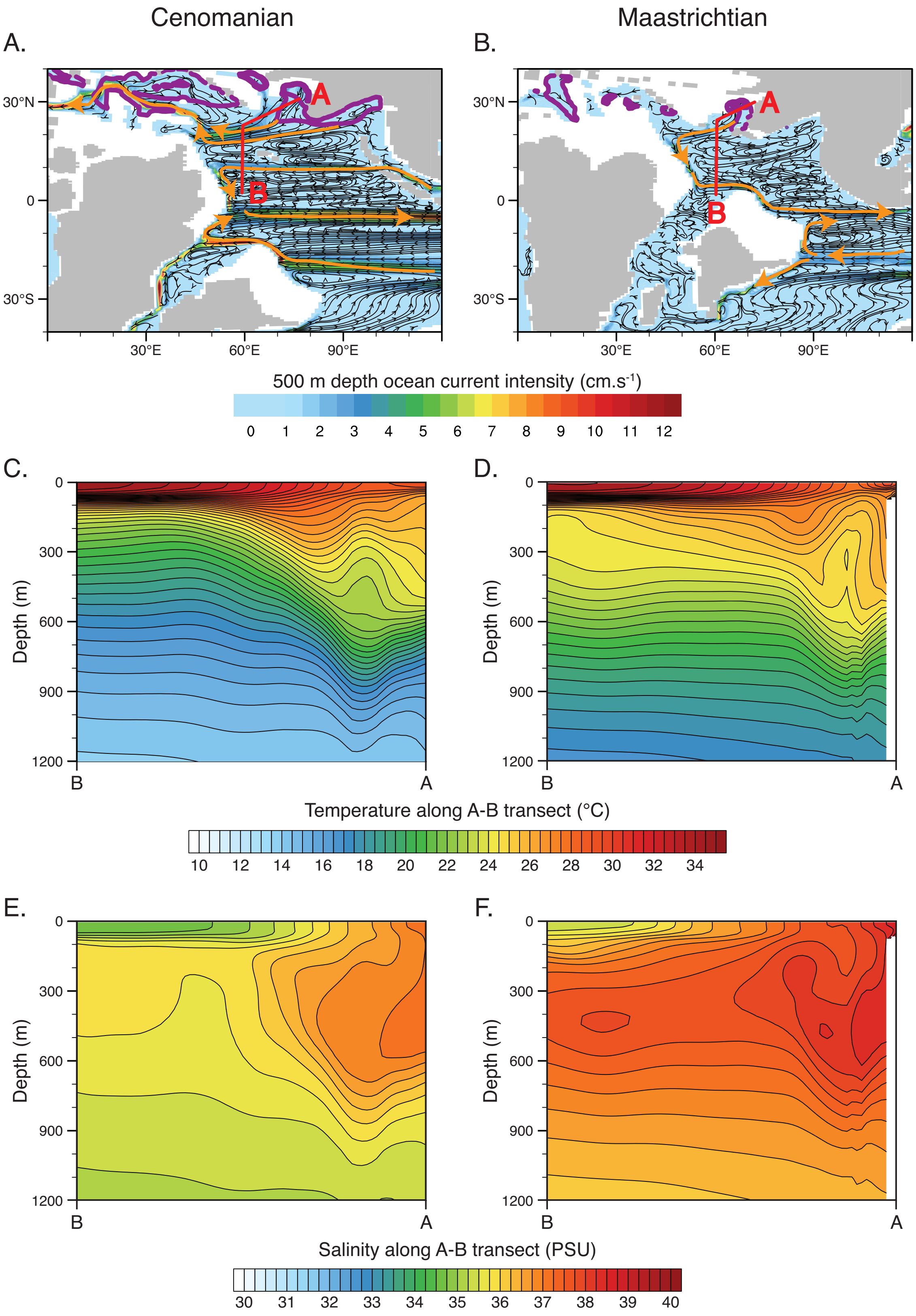

Figure S7. Upper intermediate (~ 500 m) ocean circulation for the Cenomanian (A) and Maastrichtian (B) simulations. Orange arrows represent major current systems in the northern

Indian Ocean. Purple contours represent regions of late winter deepening of the mixed layer (200 m contours). Section A-B defines an ocean transect between regions of deeper winter MLD and the central equatorial Indian Ocean. (C and D) Ocean temperatures along the A-B transect for the Cenomanian and Maastrichtian respectively. (E and F) Same as C and D for the ocean salinity.

24

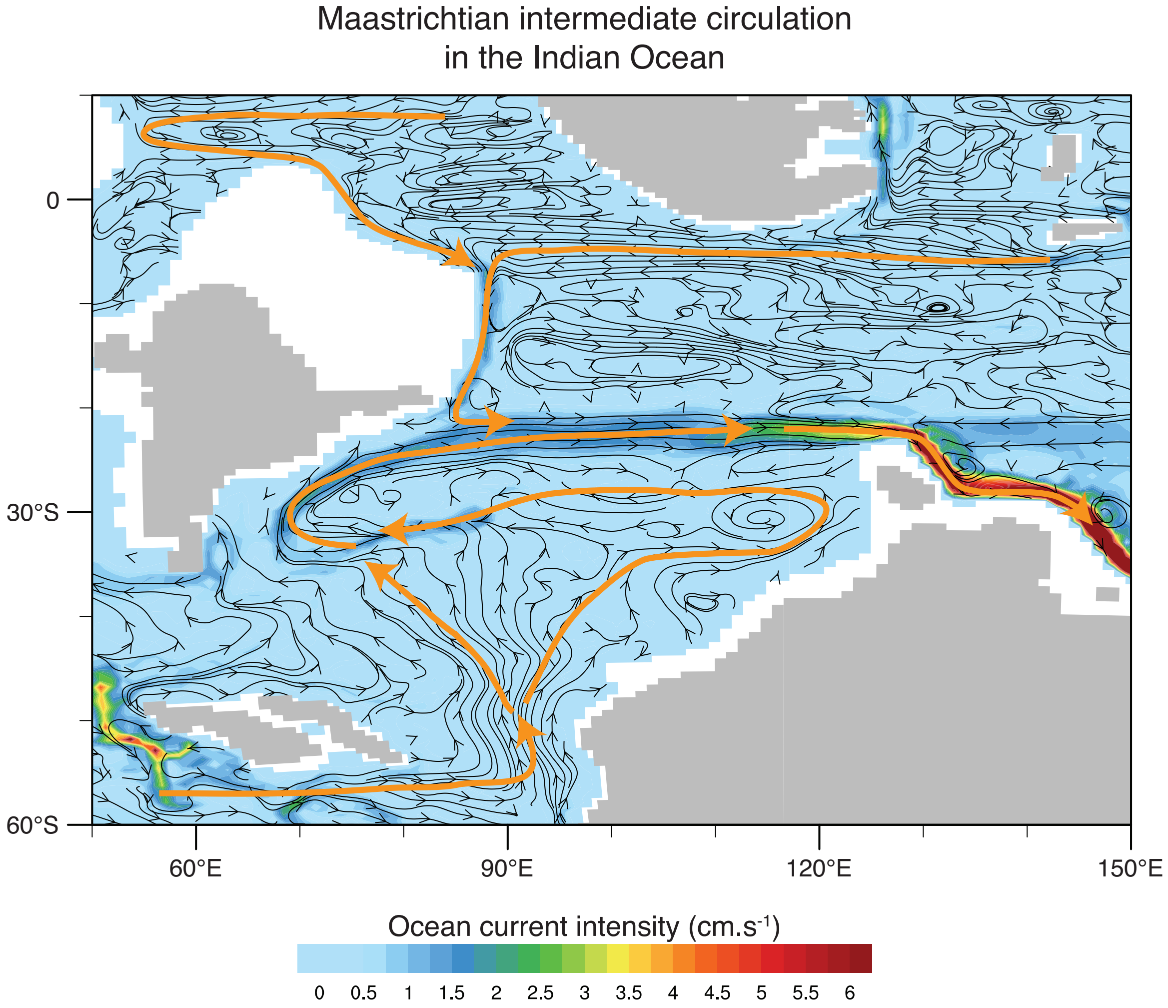

Figure S8. Maastrichtian intermediate circulation (1000 m) in the Indian Ocean. Orange arrows represent major intermediate current systems in the Indian Ocean.

25

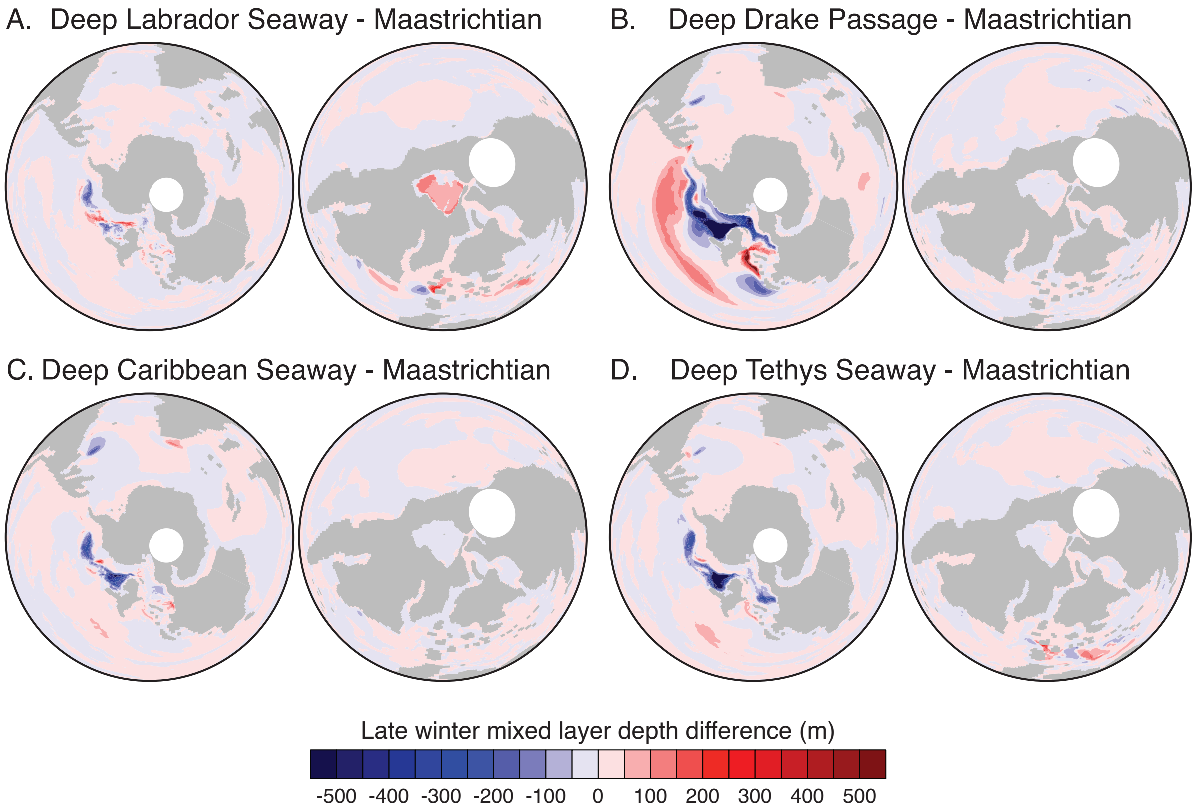

Figure S9. Southern and Northern hemispheres late winter maximal mixed layer depth difference (m) between the sensitivity experiments and the Maastrichtian simulation.

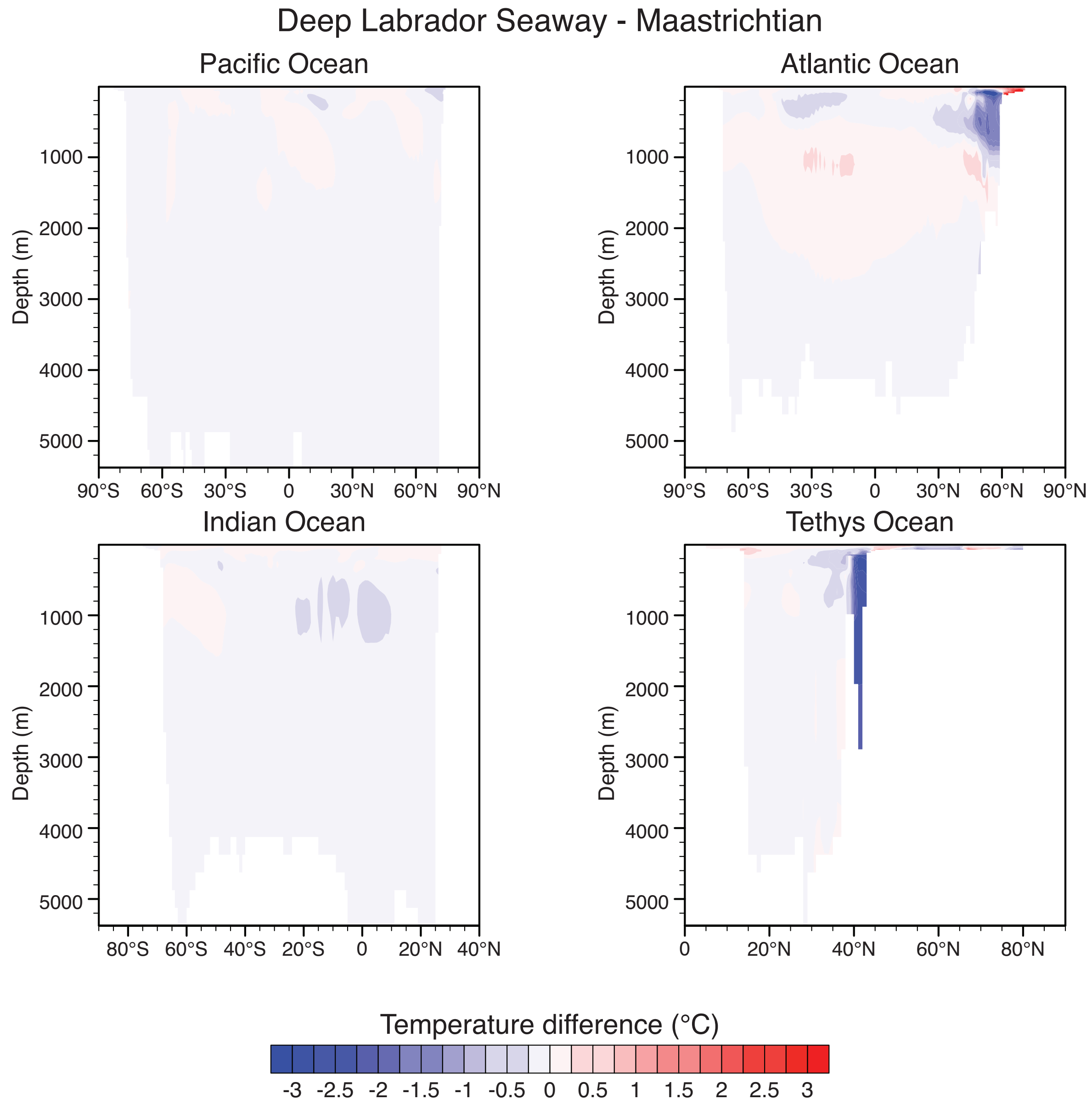

Figure S10. Zonally averaged ocean temperature changes (°C) in the different basins between the Deep Labrador Seaway and the Maastrichtian simulations.

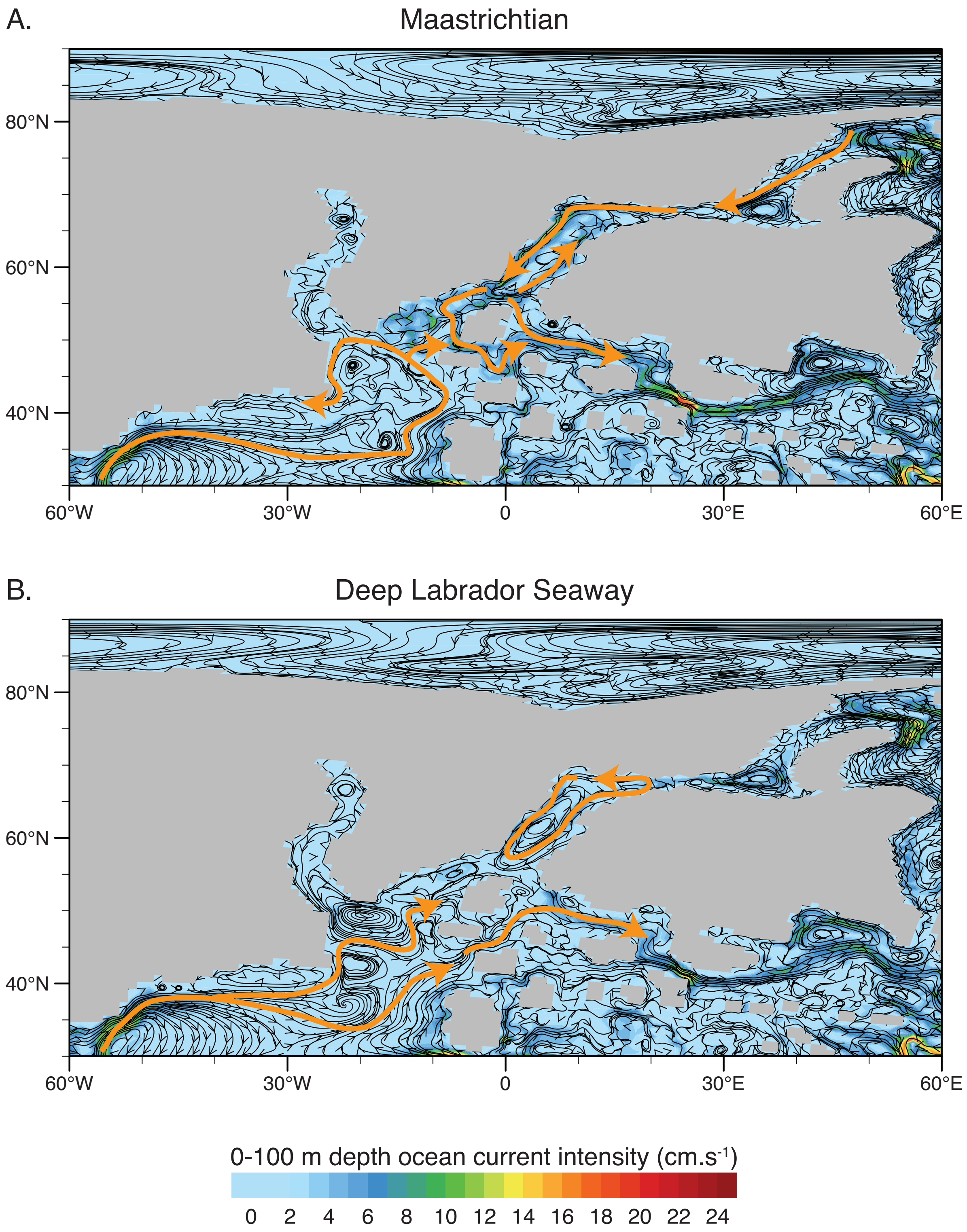

Figure S11. North Atlantic and northern Tethys upper ocean circulation in (A) the Maastrichtian and (B) the Deep Labrador Seaway experiments. Orange arrows represent major current systems.

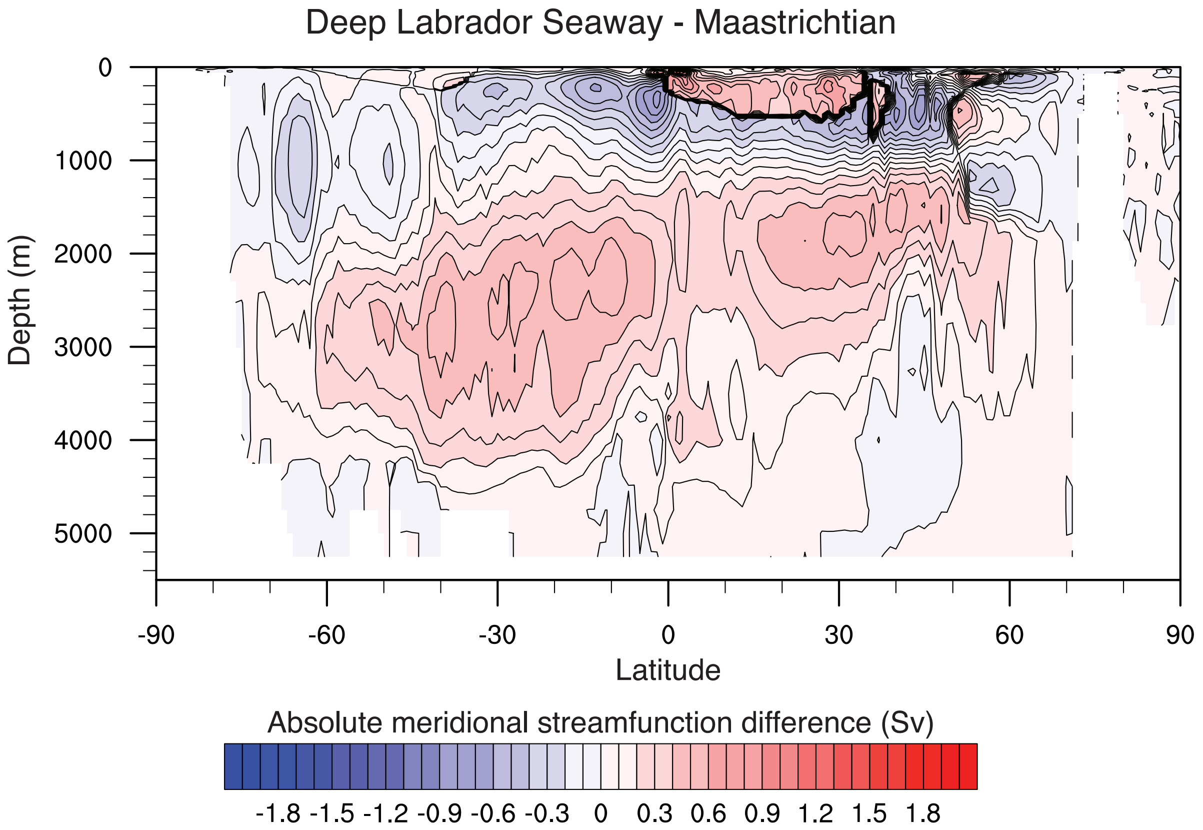

Figure S12. Difference of the absolute values of the global northward meridional streamfunction between the Deep Labrador Seaway and the Maastrichtian experiments. Positive values indicate a more vigorous circulation regardless of the sign of the global streamfunction in each simulation because the two global streamfunctions are very similar (Fig. 4B and 4C).

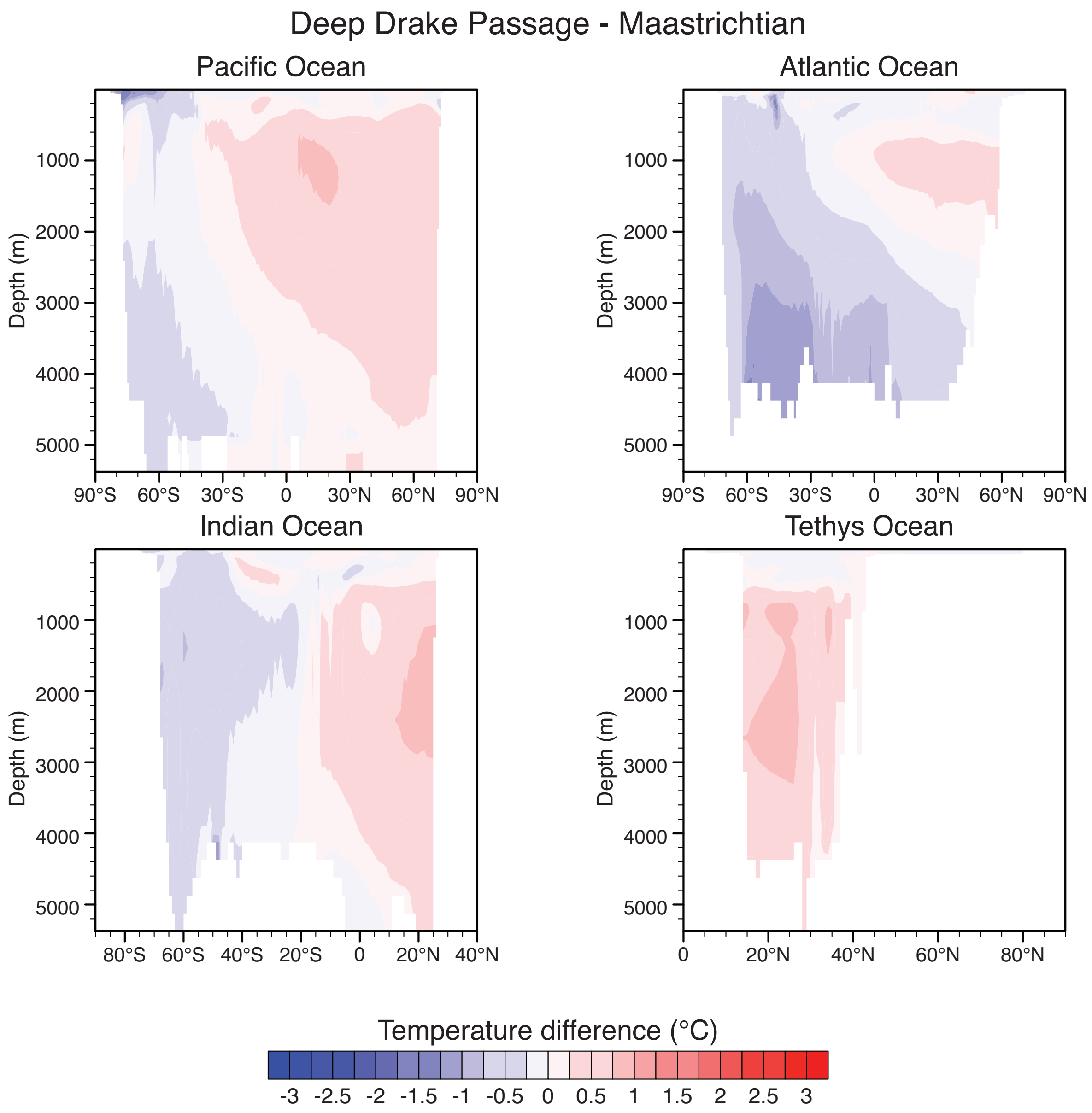

Figure S13. Zonally averaged ocean temperature changes (°C) in the different basins between the Deep Drake Passage and the Maastrichtian simulations.

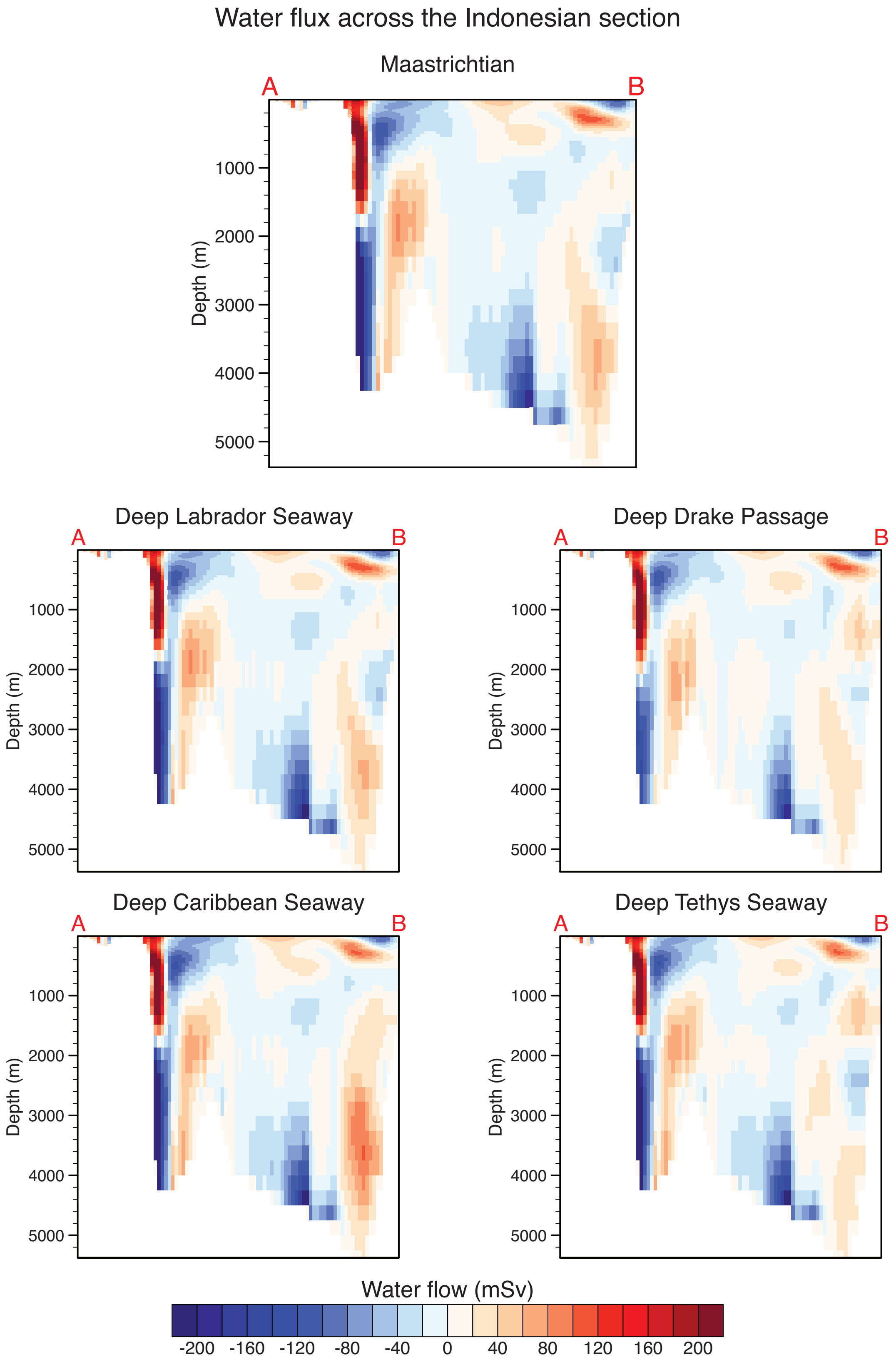

Figure S14. Water flux across the Indonesian section (mSv) for the Maastrichtian and Maastrichtian sensitivity experiments.

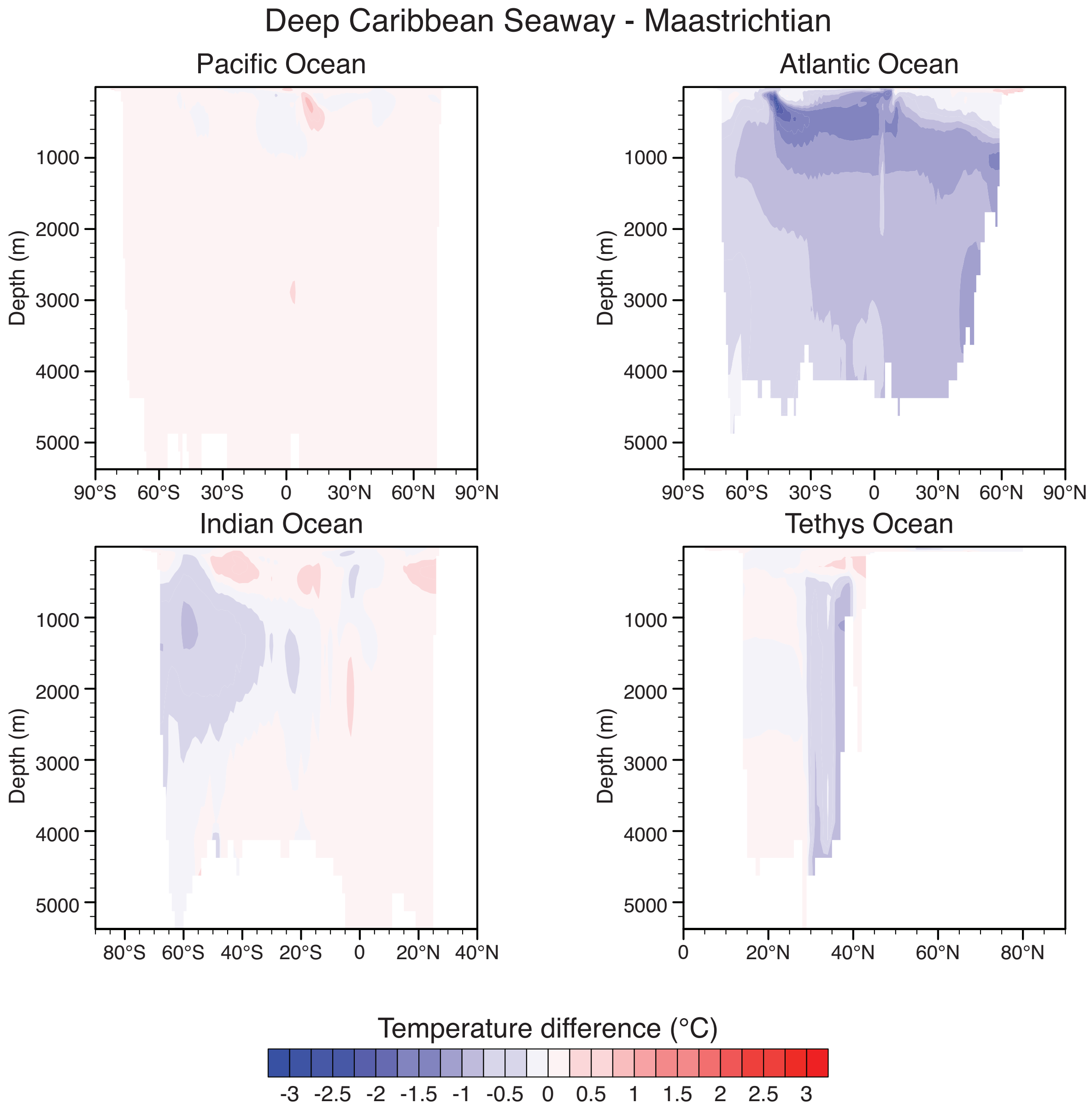

Figure S15. Zonally averaged ocean temperature changes (°C) in the different basins between the Deep Caribbean Seaway and the Maastrichtian simulations.

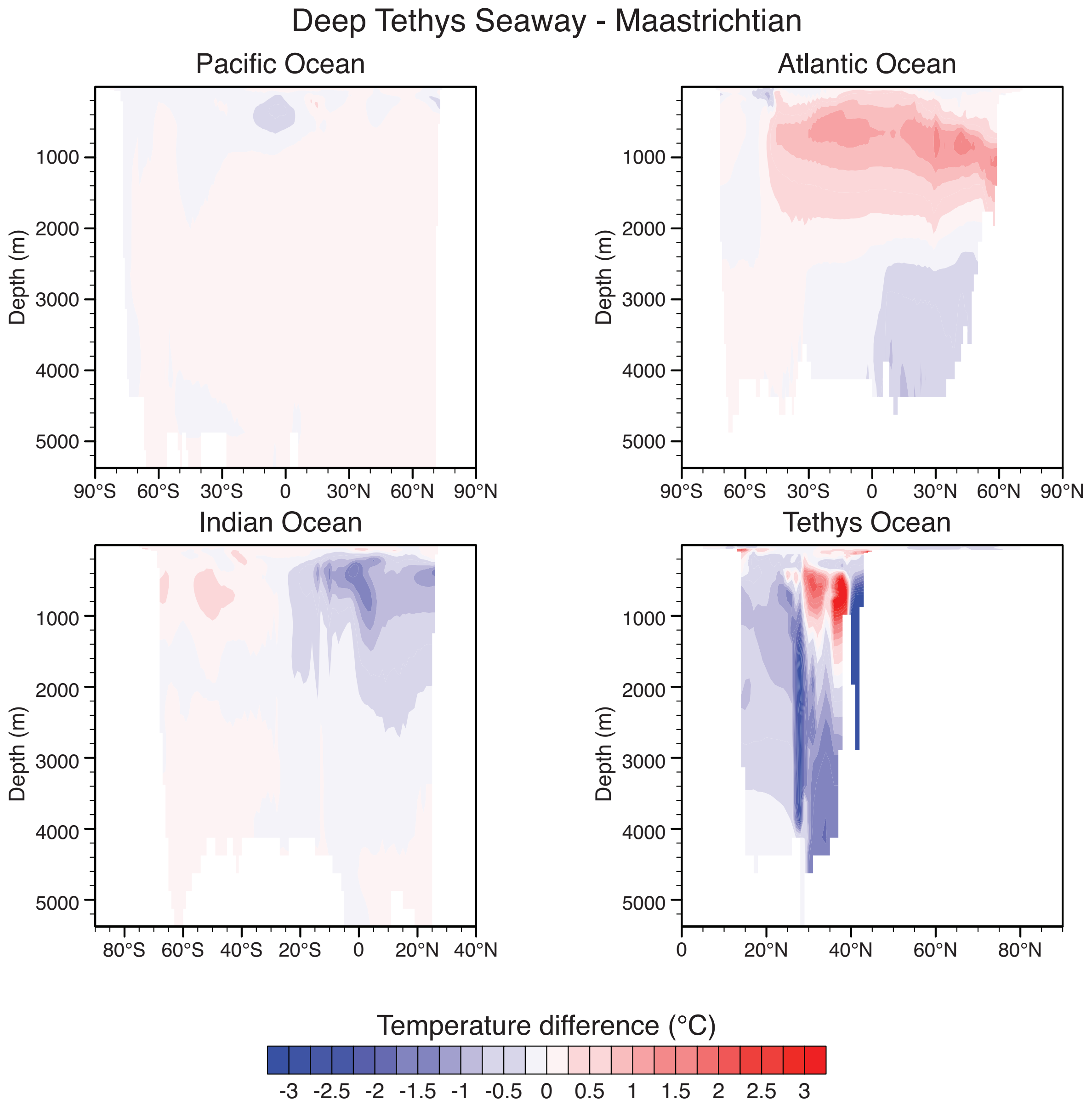

Figure S16. Zonally averaged ocean temperature changes (°C) in the different basins between the Deep Tethys Seaway and the Maastrichtian simulations.

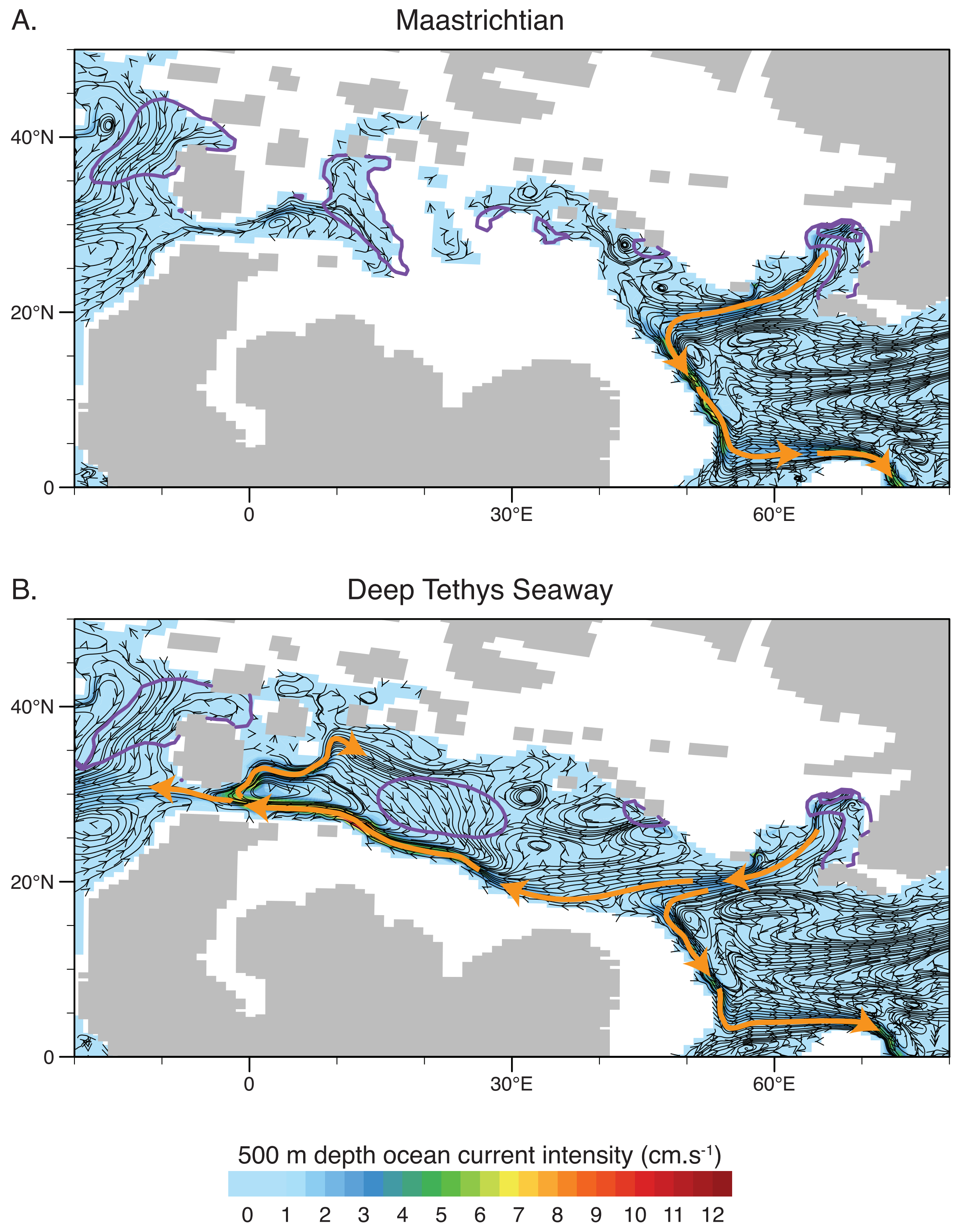

Figure S17. Tethys upper intermediate (~ 500 m) ocean circulation in (A) the Maastrichtian and (B) the Deep Tethys Seaway experiments. Orange arrows represent major current systems. Purple contours represent regions of late winter deepening of the mixed layer (200 m contours).

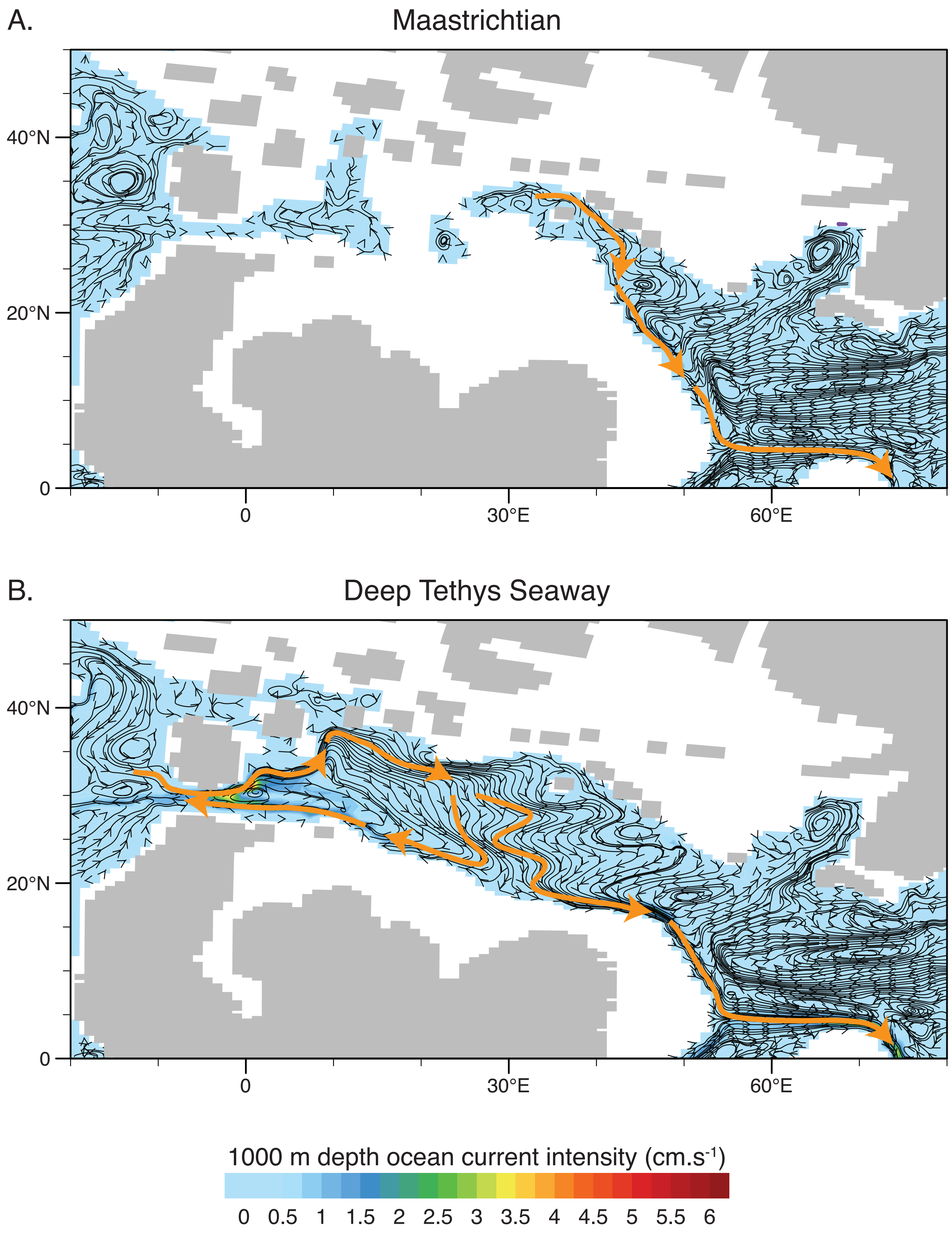

Figure S18. Tethys deep intermediate (~ 1000 m) ocean circulation in (A) the Maastrichtian and (B) the Deep Tethys Seaway experiments. Orange arrows represent major current systems.

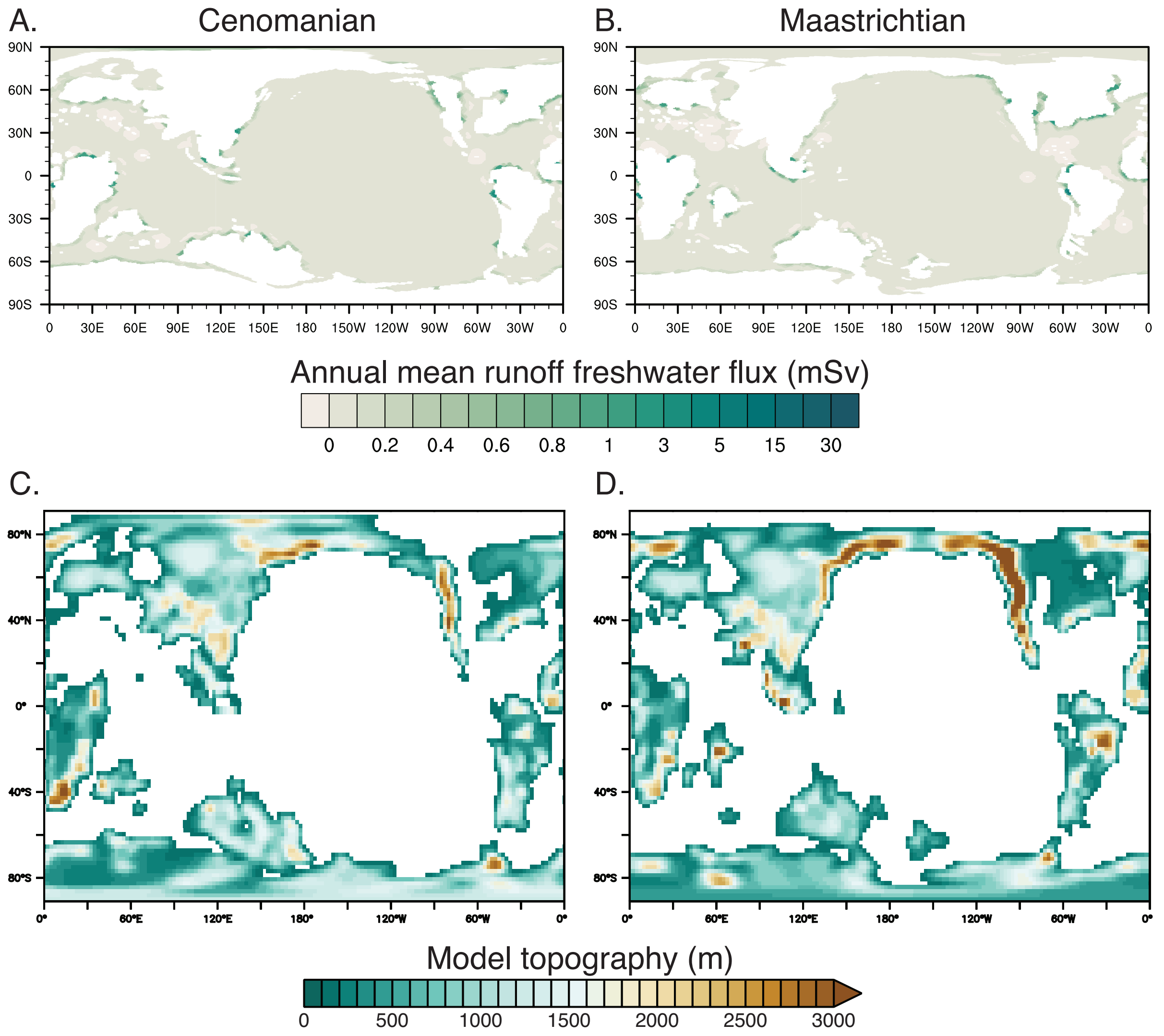

Figure S19. Annual mean runoff freshwater discharge into the ocean (mSv) for (A) the Cenomanian and (B) the Maastrichtian simulations. (C) Cenomanian topography seen by the CAM4 atmospheric model. (D) Same for the Maastrichtian.

References

Doubrovine, P. V., and Tarduno, J. A.: Late Cretaceous paleolatitude of the Hawaiian hot spot: New paleomagnetic data from Detroit Seamount (ODP Site 883), Geochemistry, Geophysics, Geosystems, 5, 2004.

Frank, T. D., Thomas, D. J., Leckie, R. M., Arthur, M. A., Bown, P. R., Jones, K., and Lees, J. A.: The Maastrichtian record from Shatsky Rise (northwest Pacific): A tropical perspective on global ecological and oceanographic changes, Paleoceanography, 20, 2005.

Gradstein, F. M., and Ludden, J. N.: 43. Legs 122 and 123, northwestern Australian margin—a stratigraphic and paleogeographic summary, Proceedings of the Ocean Drilling Program, Scientific Results, 1992, 801-816,

Hague, A. M., Thomas, D. J., Huber, M., Korty, R., Woodard, S. C., and Jones, L. B.: Convection of North Pacific deep water during the early Cenozoic, Geology, 40, 527-530, 10.1130/g32886.1, 2012.

Jiménez Berrocoso, Á., MacLeod, K. G., Martin, E. E., Bourbon, E., Londoño, C. I., and Basak, C.: Nutrient trap for Late Cretaceous organic-rich black shales in the tropical North Atlantic, Geology, 38, 1111-1114, 2010.

Le Houedec, S., Meynadier, L., Cogné, J. P., Allègre, C. J., and Gourlan, A. T.: Oceanwide imprint of large tectonic and oceanic events on seawater Nd isotope composition in the Indian Ocean from 90 to 40 Ma, Geochemistry, Geophysics, Geosystems, 13, 2012.

MacLeod, K. G., Martin, E. E., and Blair, S. W.: Nd isotopic excursion across Cretaceous ocean anoxic event 2 (Cenomanian-Turonian) in the tropical North Atlantic, Geology, 36, 811-814, 2008.

MacLeod, K. G., Londoño, C. I., Martin, E. E., Berrocoso, Á. J., and Basak, C.: Changes in North Atlantic circulation at the end of the Cretaceous greenhouse interval, Nature Geoscience, 4, 779, 2011.

Martin, E. E., MacLeod, K. G., Berrocoso, A. J., and Bourbon, E.: Water mass circulation on Demerara Rise during the Late Cretaceous based on Nd isotopes, Earth and Planetary Science Letters, 327, 111-120, 2012.

Masson, D. G., Montadert, L., and Scrutton, R. A.: Regional Geology of the Goban Spur continental margin, Initial Reports of the Deep Sea Drilling Project, 80, 1115-1139, 1985.

Moiroud, M., Pucéat, E., Donnadieu, Y., Bayon, G., Guiraud, M., Voigt, S., Deconinck, J.-F., and Monna, F.: Evolution of neodymium isotopic signature of seawater during the Late Cretaceous: Implications for intermediate and deep circulation, Gondwana Research, 36, 503-522, 2016.

Murphy, D. P., and Thomas, D. J.: Cretaceous deep-water formation in the Indian sector of the Southern Ocean, Paleoceanography, 27, PA1211, 10.1029/2011pa002198, 2012.

Murphy, D. P., and Thomas, D. J.: The evolution of Late Cretaceous deep‐ocean circulation in the Atlantic basins: Neodymium isotope evidence from South Atlantic drill sites for tectonic controls, Geochemistry, Geophysics, Geosystems, 14, 5323-5340, 2013.

Robinson, S. A., Murphy, D. P., Vance, D., and Thomas, D. J.: Formation of "Southern Component Water" in the Late Cretaceous: Evidence from Nd-isotopes, Geology, 38, 871-874, 10.1130/g31165.1, 2010.

Robinson, S. A., and Vance, D.: Widespread and synchronous change in deep-ocean circulation in the North and South Atlantic during the Late Cretaceous, Paleoceanography, 27, n/a-n/a, 10.1029/2011pa002240, 2012.

Thomas, D. J.: Evidence for deep-water production in the North Pacific Ocean during the early Cenozoic warm interval, Nature, 430, 65, 2004.

Thomas, D. J., Korty, R., Huber, M., Schubert, J. A., and Haines, B.: Nd isotopic structure of the Pacific Ocean 70–30 Ma and numerical evidence for vigorous ocean circulation and ocean heat transport in a greenhouse world, Paleoceanography, 29, 454-469, 2014.

Voigt, S., Jung, C., Friedrich, O., Frank, M., Teschner, C., and Hoffmann, J.: Tectonically restricted deep-ocean circulation at the end of the Cretaceous greenhouse, Earth and Planetary Science Letters, 369, 169-177, 2013.